Pressure-dependent luminescence spectroscopy of molybdenum(IV) oxo complexes†

Etienne Lanthier,[a] Jesper Bendix*[b] and Christian Reber*[a]

Received 18th November 2009, Accepted 4th February 2010
First published as an Advance Article on the web 8th March 2010
DOI: 10.1039/b924242b

Luminescence spectra are reported for *trans*-[MoOCl(CN-*t*-Bu)$_4$]BPh$_4$ and *trans*-[MoOF(pyridine)$_4$]BPh$_4$. The maxima of the broad luminescence bands are at energies of 12000 and 13000 cm^{-1}, respectively. Resolved vibronic structure involves the metal-oxo stretching mode with a vibrational frequency of approximately 950 cm^{-1} (Raman) in both compounds. The pressure behavior of the luminescence bands shows a distinct difference: a blue shift of +12 cm^{-1} kbar^{-1} is observed for [MoOCl(CN-*t*-Bu)$_4$]BPh$_4$, and a red-shift of -8 cm^{-1} kbar^{-1} is obtained for [MoOF(pyridine)$_4$]BPh$_4$. At pressures above 25 kbar, the luminescence maximum of [MoOCl(CN-*t*-Bu)$_4$]BPh$_4$ shows a change from a blue-shift to a red-shift and the Raman peak corresponding to the metal-oxo stretching mode at 954 cm^{-1} becomes broad and its maximum decreases with increasing pressure, leading to a strong deviation from the linear increase of +0.24 cm^{-1} kbar^{-1} observed at pressures below 25 kbar. These unusual pressure effects are rationalized in terms of the influence of pressure on the metal–ligand bonds and oxo-metal–ligand angles using DFT calculations.

1. Introduction

Transition metal complexes with metal-oxo bonds have a rich variety of excited-state properties, extensively probed in the past mainly for metals of the 5d series.[1-11] One of the key aspects of their low-energy electronic transitions is the influence of strong spin–orbit coupling between the ground state and excited states of identical symmetry, leading to distinct vibronic signatures.[8,10] Under external pressure, the luminescence band maxima of *trans*-dioxo complexes show a red shift and changes in the intensity distribution within the high-frequency vibronic progression involving the symmetric metal-oxo stretching mode,[9,10,12] whose frequency shows a linear increase with pressure.[13] All these pressure effects are reversible and have been analyzed quantitatively.[9,10,12] Complexes of 5d metals with only a single metal–ligand multiple bond to a nitrido ligand have shown particularly intriguing luminescence properties with detailed spectra dominated by progressions in the high-frequency stretching mode involving the multiple bond.[14,15] Luminescence from compounds with a single metal-oxo multiple bond often occurs at low energy in the near-infrared region.[16-18] To the best of our knowledge, no pressure-dependent luminescence spectra of complexes with a single metal–ligand multiple bond have been reported. Pressure-dependent Raman spectra of two mono-oxo complexes of rhenium(V)[13] have shown a surprising deviation from the linear increase always observed for the metal-oxo stretching frequency of *trans*-dioxo complexes.[9,10,12] At pressures higher than 20 to 30 kbar, the observed frequency for these two complexes remains constant or decreases as a function of pressure, a reversible effect that could not be analyzed from the Raman spectra, but will be discussed based on the luminescence and Raman results presented in the following.

Metal-oxo complexes of 4d metals have received less attention, but several reports on their electronic spectroscopy have been published.[17,18] Detailed luminescence spectra of *trans*-dioxo technetium(V) complexes show the most highly resolved vibronic structure reported for 4d metal-oxo complexes,[19] and detailed spectra of molybdenum(IV) nitrido complexes have also been reported.[20]

Molybdenum(IV) oxo complexes are important species at the active sites of enzymes catalyzing oxygen atom transfer reactions.[21] They provide an attractive new area to explore, as spin–orbit coupling is expected to have a smaller influence on their spectroscopic properties than for 5d metal centers. These complexes with the d^2 electron configuration have been studied by visible absorption and luminescence spectroscopy, with luminescence spectra that are often incomplete due to instrumental limitations.[17,18]

We present luminescence spectra of the two d^2 configured molybdenum(IV) oxo complexes [MoOCl(CN-*t*-Bu)$_4$]$^+$ and [MoOF(pyridine)$_4$]$^+$ illustrated in Scheme 1.

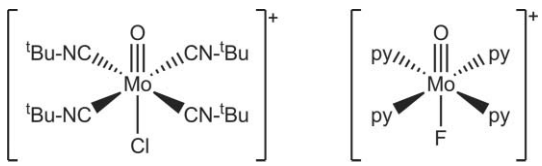

Scheme 1 Schematic structures of [MoOCl(CN-*t*-Bu)$_4$]$^+$ and [MoOF(pyridine)$_4$]$^+$

[a]*Département de chimie, Université de Montréal, Montréal, QC H3C 3J7, Canada. E-mail: christian.reber@umontreal.ca*
[b]*Department of Chemistry, H. C. Ørsted Institute, University of Copenhagen, Universitetsparken 5, DK-2100, Copenhagen, Denmark. E-mail: bendix@kiku.dk*

† Electronic supplementary information (ESI) available: Absorption spectra, luminescence lifetimes, temperature and pressure-dependent Raman and luminescence spectra and selected DFT calculations for [MoOCl(CN-*t*-Bu)$_4$]BPh$_4$ and [MoOF(pyridine)$_4$]BPh$_4$. CCDC reference number 764168. For ESI and crystallographic data in CIF or other electronic format see DOI: 10.1039/b924242b

The complexes have different ligands in the xy plane perpendicular to the Mo–oxo multiple bond, which is oriented parallel to the molecular z axis throughout the following. The isocyanide ligands are π-acceptors, whereas the pyridine ligands are expected to be π-donors, as determined from the comparison of ground- and emitting state vibronic intervals in luminescence and absorption spectra of *trans*-dioxo complexes of rhenium(V).[2,7,8] In the *trans* position to the oxo ligand, chloro and fluoro ligands are explored. Luminescence spectra for both compounds are observed in a similar energy range between approximately 8000 cm^{-1} and 14000 cm^{-1}. Despite these similarities, the ground- and emitting state characteristics vary considerably, as is shown in the following by pressure-dependent luminescence spectra. $[MoOCl(CN\text{-}t\text{-}Bu)_4]^+$ is the first metal-oxo complex for which a blue shift of the luminescence band maximum is observed with pressure, in contrast to $[MoOF(pyridine)_4]^+$, where a pressure-induced red shift comparable to those reported for *trans*-dioxo complexes of rhenium(V) is observed. A surprising observation is the change from a blue-shift to a red-shift of the band maximum for $[MoOCl(CN\text{-}t\text{-}Bu)_4]^+$ at pressures on the order of 25 kbar. This wide variety of pressure-induced spectroscopic effects shows the important influence of all metal–ligand bonds in mono-oxo complexes. Theoretical electronic structure calculations on a variety of $E{=}ML_4X$ complexes with one E=M multiple bond *trans* to the M-X single bond indicate that the E=M–L angle decreases if the M-X bond *trans* to the multiple bond is shortened.[22-25] External pressure provides an experimental approach to the study of such effects and their influence on the electronic structure.

2. Experimental

2.1 Synthesis

***trans*-[MoOCl(CN-*t*-Bu)$_4$]BPh$_4$.** $MoCl_5$, *t*-butylisocyanide and $NaBPh_4$ were purchased from Aldrich and used without any further purification. Dry methanol was deoxygenated with nitrogen for 30 min. All other solvents were distilled according to standard procedures and purged with N_2. All syntheses were done under N_2 atmosphere using Schlenk techniques. The complex $[MoOCl(CN\text{-}t\text{-}Bu)_4]BPh_4$ was synthesized following published procedures[17,18] and characterized by ^1H and ^{13}C NMR spectroscopy.[17] Its crystal structure has been reported.[18] Crystals with diameters of a few mm were obtained within 2 days from a saturated dichloromethane solution stored at –20 °C.

***trans*-[MoOF(pyridine)$_4$]BF$_4$.** $Na_3[Mo(HCOO)_6]$ was prepared according to the literature method.[26] Pyridine, tetrafluoroboric acid, and sodium tetraphenylborate was obtained commercially (Sigma-Aldrich) and used as received.

NMR spectra were recorded on a Varian UNITY 400 spectrometer. Infrared spectra were recorded on a solid sample (KBr disk) on a Perkin-Elmer 2000 FT-IR/FT-NIR Raman spectrometer. Molybdenum was analyzed spectroscopically as the thiocyanatecomplex formed after oxidative degradation. Elemental analyses(C, H, and N) were performed at the Micro Analytical Laboratory at the Department of Chemistry, University of Copenhagen with a CE Instruments Flash 112 series EA.

$Na_3[Mo(HCOO)_6]$ (9.4 g; 21 mmol) was dissolved in a mixture of neat pyridine (60 ml) 50% aqueous HBF_4 (30 ml) and water (30 ml). The stirred solution was heated to 70 °C for 15 min. The reaction mixture, which during the heating had turned from light yellow to very dark green, was diluted with 40 ml of water and left over night at 5 °C. The first crop of crystals was filtered off and washed with ice cold water and diethylether : THF (40 : 1). Yield 4.1 g (36%). The filtrate was diluted with another 60 ml of water and left at 5 °C for another 24h. Filtering and washing as above yielded another 1.8 g (16%) of product. The tetrafluoroborate salt is soluble in pyridine, acetone and moderately soluble in THF. It dissolves in water with decomposition. The product can be reprecipitated by adding to a saturated pyridine solution a 10 fold volume of 0.5 M aqueous HBF_4.

Analysis: Calculated for $C_{20}H_{20}BN_4OF_5Mo$: H: 3.77%; C: 44.97%; N: 10.49%; Mo: 18.03%. Found: H: 3.78%; C: 44.99%; N: 10.38%; Mo: 18.64%. Redox titration with basic $[Fe(CN)_6]^{3-}$ yielded an average molybdenum oxidation state of 4.12. IR: ν(Mo–O): 953 cm^{-1}. Diamagnetism of the compound was confirmed by sharp, unshifted NMR spectra ($^{13}C\{^1H\}$ NMR: $\delta = 125.45$ ppm, 139.265 ppm, and 147.703 ppm for o-, m-, and p-positions of the coordinated pyridines, respectively).

X-ray crystallography. Crystal structure and refinement data for *trans*-$[MoOF(py)_4](BPh_4)\cdot 0.64\ CH_3OH$ are summarized in Table 1. Details of the structure determination are available in the Electronic Supplementary Information as a cif file. All non hydrogen atoms were refined with anisotropic temperature factors. From the diffraction data, an orientational disorder along the O–Mo–F axis was evident as previously observed for related phosphine complexes,[27,28] and it was modeled in the same way. The molecular structure diagrams were made with the ORTEP-II program.[29] Crystals suitable for X-ray diffraction were obtained

Table 1 Crystallographic Data for *trans*-$[MoOF(py)_4](BPh_4)\cdot 0.64\ CH_3OH$

trans-$[MoOF(py)_4](BPh_4)\cdot 0.64\ CH_3OH$	
empirical formula	$C_{44.64}\ H_{42.56}\ BFMoN_4O_{1.64}$
fw/g mol^{-1}	787.03
T/K	122(1)
wavelength/Å	0.71073
Space group	$P2_1/c$ (No. 14)
Crystal size/mm	$0.300 \times 0.123 \times 0.081$
unit cell dimensions	
a/Å	13.4721(17)
b/Å	10.8240(9)
c/Å	26.9439(18)
α (°)	90.000
β (°)	102.952(8)
γ (°)	90.000
V/Å^3	3829.0(6)
Z	4
d_c/g cm^{-3}	1.365
$F(000)$	1584
(range for data collection (°)	1.55–27.46
no. reflections coll.	80472
no of unique Reflections, R_{int}	8759, 0.0321
no of data/restraints/params	7830/3/516
Final R_1, wR_2	
$[I > 2\sigma(I)]$ [a]	0.0626, 0.1193
Final R_1, wR_2	
(all data)[a]	0.0721, 0.1228
Goodness-of-fit on F^2	1.305

[a] $R_1 = \Sigma \parallel F_o \mid - \mid F_c \parallel / \Sigma \mid F_o \mid$; $wR_2 = [\Sigma\{w(\mid F_o \mid^2 - \mid F_c \mid^2)^2\}/\Sigma\{w(\mid F_o \mid^2)^2\}]^{1/2}$.

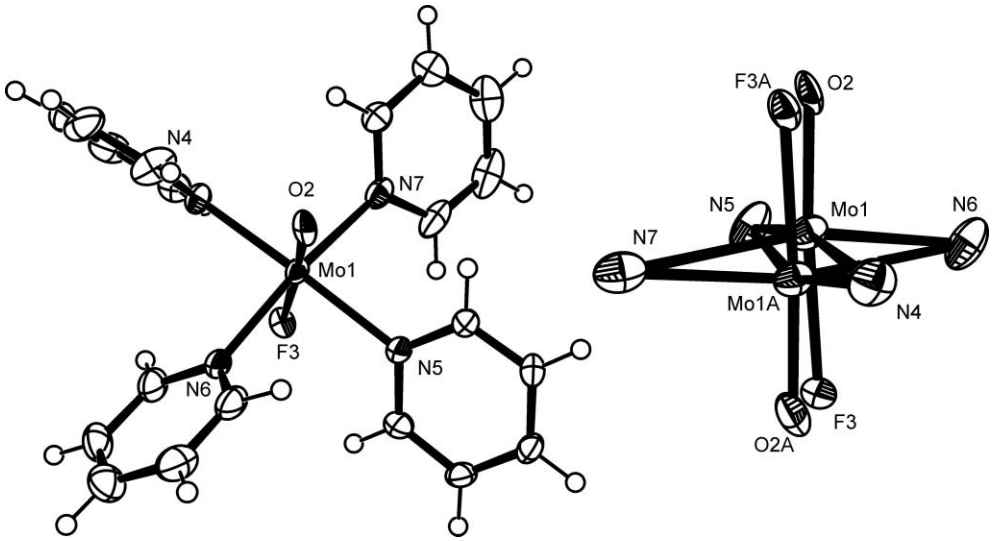

Fig. 1 Structure of the cation in *trans*-[Mo(O)F(pyridine)$_4$](BPh$_4$)·0.64 CH$_3$OH. The structure was refined with an orientational disorder of the O–Mo–F axis (right) with almost equal population of the two orientations (0.473/0.527) and very similar geometries of ions with the two disordered orientations. Important bond distances and angles are summarized in Table 2.

Table 2 Selected Bond Lengths (Å) and Angles (deg.) for *trans*-[Mo(O)F(py)$_4$](Bph$_4$)·0.64 CH$_3$OH

Mo1–O2	1.670(15)	Mo1A–O2A	1.664(13)
Mo1–F3	2.011(12)	Mo1A–F3A	2.026(11)
O2–Mo1–F3	175.7(6)	O2A–Mo1A–F3A	175.7(6)
Mo1–N4	2.187(2)	Mo1–N6	2.109(3)
Mo1–N5	2.188(3)	Mo1–N7	2.293(3)
O2–Mo1–N4	93.9(6)	O2–Mo1–N6	96.7(5)
O2–Mo1–N5	97.9(7)	O2–Mo1–N7	99.3(4)

by letting a concentrated solution of the tetrafluoroborate salt in methanol containing a few drops of pyridine diffuse together with a methanolic solution of sodium tetraphenylborate. This affords dark green block shaped crystals in 24 h.

Fig. 1 illustrates the cation and relevant bond lengths and angles are summarized in Table 2.

2.2 Spectroscopic techniques

Luminescence spectroscopic measurements were carried out with two different instruments. The first is a Renishaw System 3000 microscope spectrometer used to collect both Raman and luminescence spectra. The samples were cooled in a He gas flow microcryostat (Janis ST-500) used for temperatures down to 10 K. The 514.5 nm line of an argon ion laser (power *ca.* 2 mW) and the 632.8 nm line of a He–Ne laser (power *ca.* 4 mW) were used as excitation sources and focused onto the sample. The light was collected and detected with a Peltier-cooled CCD camera. The second instrument to measure luminescence spectra is a single-channel scanning spectrometer. A continuous flow helium cryostat (Oxford Instruments CF 1204) was used to cool samples down to 15 K. The excitation wavelength was again 514.5 nm (Spectra Physics Stabilite 2017). The excitation light was focused onto the samples with a quartz lens and the luminescence collected at 90° by a spherical mirror, then dispersed through a computer-controlled 0.5 m monochromator (Spex 500M, 600 lines/mm grating) with a long-pass filter (Schott RG 645) positioned at the entrance slit. Luminescence was detected either with a cooled photomultiplier tube (Hamamatsu R406/Products for Research TE 177RF cooler) or germanium photodiode (Applied Detector Corporation 403 UL, cooled with liquid nitrogen) connected to a lock-in amplifier (Stanford Research Systems SR 830) with the luminescence signal modulated with an optical chopper (Stanford Research Systems SR 540). The response characteristics of all detectors vary strongly over the wavelength range of interest. All luminescence spectra were corrected for instrument response by calibration with a tungsten lamp[30] and we obtained identical corrected spectra in the overlapping wavelength range of the two instruments.

Pressure-dependent luminescence and Raman spectra were recorded using the microscope system described above. Pressure was applied to the solid samples by loading crystals into a gasketed diamond-anvil cell (DAC, High-Pressure Diamond Optics). Small ruby chips were added to the sample cell and their luminescence (R_1 line, 694.2 nm) was used to calibrate pressures.[31] Paraffin oil was the pressure-transmitting medium.

Temperature-dependent luminescence lifetimes were measured using the doubled output (532 nm) of a Nd:YAG pulsed laser (Continuum Mini-Lite II, ~ 5 ns pulse width). The luminescence was collected by the single-channel system described above using the R406 photomultiplier. The signal was averaged and saved on a digital oscilloscope (Tektronix TDS 380) triggered by a photodiode (Thorlabs FDS 100). Luminescence lifetimes were recorded at multiple wavelengths as a function of temperature. All decay traces were fitted with double exponential functions. The shortest lifetime, representing 1% of the signal, is assigned to resistor (1 kΩ) unload.

Absorption measurements were carried out with a Varian Cary 5E spectrometer. Crystals were mounted to minimize the amount of stray light and were cooled down to 15 K using the same He gas flow cryostat described above for the luminescence lifetime measurements.

DFT calculations were made with the Gaussian 01 (2001) program package.[32] Crystallographic atom coordinates from this

work and from the literature[18] were used as a starting point and first optimized with the SVWN local approximation, followed by the PBE functional for tighter geometry optimization and calculation of vibrational frequencies. The lanl2dz basis set was used for all the calculations. A recent theoretical study on a series of metal-oxo complexes has shown that different functionals lead to identical lowest-energy electronic transitions and that the choice of a specific functional is not critical for this category of compounds.[33]

3. Spectroscopic results

Absorption spectra of many d^2 oxo complexes show two broad, weak absorption bands in the visible wavelength range, corresponding to the lowest-energy spin-forbidden and spin-allowed d-d transitions.[3,7,8] The lowest-energy absorption band of crystalline [MoOCl(CN-*t*-Bu)$_4$]BPh$_4$ measured at low temperature is identical to the literature data[18] and shown in Fig. S1, ESI,† in comparison to the luminescence spectrum. This comparison indicates that d–d transitions are observed in absorption and luminescence. The ground and emitting state electron configurations for the luminescence transition are $(d_{xy})^2$ and $(d_{xy})^1(d_{xz,yz})^1$, respectively.[2,3,33] The full luminescence spectrum of [MoOCl(CN-*t*-Bu)$_4$]BPh$_4$ at 15 K is shown in Fig. 2. Its high-energy region is identical to the partial spectra reported for this complex before.[17,18] The band maximum is at approximately 12000 cm^{-1}, lower in energy by several thousand wavenumbers than the maxima for *trans*-dioxo complexes of rhenium(V). A dominant vibronic progression with an average progression interval of 920 cm^{-1} is well resolved. This interval is close to the molybdenum(IV)-oxo stretching frequency of 954 cm^{-1} determined from the Raman spectrum. The luminescence lifetime at 80 K is 43 μs, it decreases to 24 μs at room temperature. Lifetimes measured at four different wavelengths across the luminescence spectrum show a variation of less than 1 μs, as illustrated in Fig. S1, ESI.† These long lifetimes indicate that a spin-forbidden d–d luminescence transition is observed, in agreement with literature assignments based on absorption spectra, where a spin-allowed ligand-field band is observed at 549 nm with a molar absorptivity ε of 115 M^{-1}cm^{-1} in CH_2Cl_2 solution.[18] The absorption spectrum of [MoOF(pyridine)$_4$]$^+$ in $CHCl_3$ shows a broad, featureless absorption at 635 nm ($\varepsilon = 710$ m^{-1}cm^{-1}) followed by a very intense and fairly sharp MLCT transition at 422 nm ($\varepsilon = 22300$ M^{-1}cm^{-1}), responsible for the intense color of the compound. The assignment of the latter band as a MLCT is in accordance with the assignment made for the spectrum of *trans*-[Re(O)$_2$(py)$_4$]$^+$[34] and the fact that the corresponding band in the analogous tungsten complex is red-shifted by approximately 3200 cm^{-1}.[35] The luminescence spectrum of [MoOF(pyridine)$_4$]BPh$_4$ is shown in Fig. 3. Its maximum is at 13000 cm^{-1}, similar in energy to [MoOCl(CN-*t*-Bu)$_4$]BPh$_4$. The vibronic structure is more complicated with average intervals of approximately 475 and 950 cm^{-1}. The higher-energy spacing corresponds to the molybdenum(IV)-oxo mode, observed at 953 cm^{-1}, a value identical within experimental precision to that observed for [MoOCl(CN-*t*-Bu)$_4$]BPh$_4$. These identical frequencies and very similar average molybdenum(IV)-oxo bond lengths of 1.67 Å, Table 2, and 1.73 Å[18] in [MoOF(pyridine)$_4$]BPh$_4$ and [MoOCl(CN-*t*-Bu)$_4$]BPh$_4$, respectively, indicate strong similarities in metal oxo bonding for the two compounds. Raman frequencies of importance to the observed vibronic structure of the luminescence spectra and assignments based on DFT calculations are given in Table 3 for both compounds.

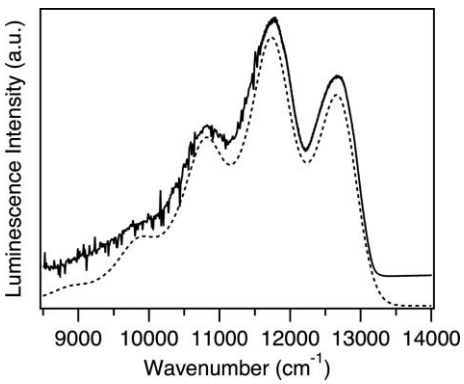

Fig. 2 Corrected luminescence spectrum of [MoOCl(CN-*t*-Bu)$_4$]BPh$_4$ at 15 K (solid line) and calculated spectrum (dotted line).

Table 3 Raman frequencies and assignments. All values are given for room temperature. Pressure-induced frequency changes are given in parentheses where available

[MoOCl(CN-*t*-Bu)$_4$]BPh$_4$	Observed frequency/cm^{-1}	Calculated frequency/cm^{-1}
Mo–oxo	954 (+0.24 cm^{-1} kbar^{-1})	947
Mo–isocyanide	441 (+0.36 cm^{-1} kbar^{-1})	441
Mo–Cl	255, 274 (shoulder), 315	277
[MoOF(pyridine)$_4$]BPh$_4$		
Mo–oxo	953 (+0.18 cm^{-1} kbar^{-1})	954
Mo–pyridine		192
Mo–F	475	478

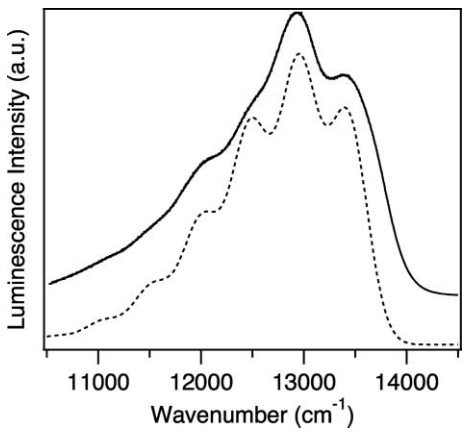

Fig. 3 Corrected luminescence spectrum of [MoOF(pyridine)$_4$]BPh$_4$ at 80 K (solid line) and calculated spectrum (dotted line).

Pressure-dependent spectroscopy provides more insight on metal–ligand bonding of the compounds in Scheme 1 and allows a detailed comparison with previously studied oxo and *trans*-dioxo complexes of rhenium(V). Fig. 4 shows the Raman spectra in the region of the metal-oxo stretching mode as a function of external pressure. Steady increases by +0.24 and +0.18 cm^{-1} kbar^{-1} are observed for [MoOCl(CN-*t*-Bu)$_4$]BPh$_4$ in Fig. 4a and [MoOF(pyridine)$_4$]BPh$_4$ in Fig. 4b, respectively, between ambient pressure and 25 kbar. The linear frequency increases for both compounds are smaller by approximately a factor of two than for *trans*-dioxo complexes, and similar to those reported for

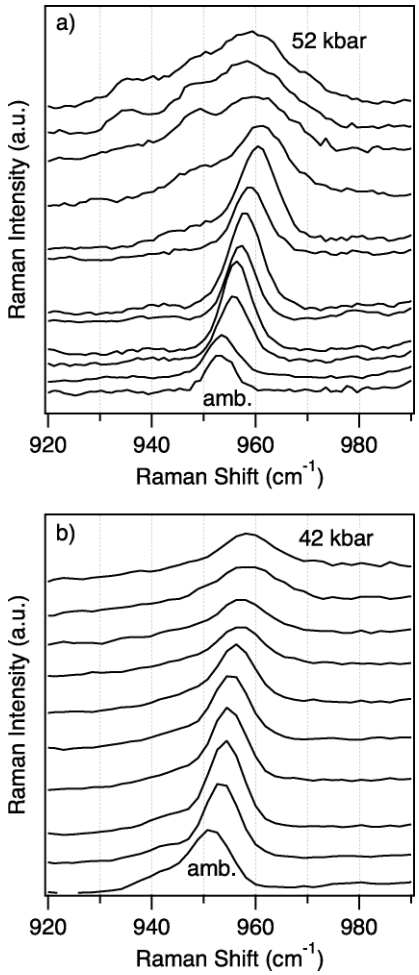

Fig. 4 Pressure-dependent Raman frequency of the Mo–oxo stretching mode at room temperature. (a) $[MoOCl(CN\text{-}t\text{-}Bu)_4]BPh_4$. Pressures (from bottom trace): ambient, 12, 13, 16, 18, 21, 25, 29, 31, 35, 40, 52 kbar. (b) $[MoOF(pyridine)_4]BPh_4$. Pressures (from bottom trace): ambient, 12, 19, 23, 26, 30, 33, 36, 39, 43 kbar.

mono-oxo complexes of rhenium(V).[13] At pressures above 25 kbar, the frequency increase continues steadily for $[MoOF(pyridine)_4]BPh_4$, but for $[MoOCl(CN\text{-}t\text{-}Bu)_4]BPh_4$ a different behavior is observed: the frequency increase of the most intense maximum does not continue and significant Raman intensity is observed lower in energy than the ambient-pressure Mo–oxo stretching frequency. The Raman signal in the molybdenum(IV)-oxo region becomes broad at pressures above 30 kbar, most likely due to pressure-induced inhomogeneity, but it is most important to point out that all pressure-induced Raman features are lower in frequency than the value for the maximum observed at 25 kbar. No other Raman bands of either compound show a corresponding non-linear change with pressure, as documented for selected Raman bands in Fig. S2, ESI.† Qualitatively similar pressure effects on the metal-oxo stretching mode have been reported for two mono-oxo complexes of rhenium(V) with chloro and bromo ligands *trans* to the oxo ligands,[13] a structural motif similar to $[MoOCl(CN\text{-}t\text{-}Bu)_4]^+$. In these compounds, the rhenium(V)-oxo Raman frequency increases with pressure up to approximately 30 kbar, then decreases, again a reversible effect observed only for this particular Raman band.[13] No analysis of the pressure-induced decrease of the rhenium(V)-oxo Raman frequency was possible, in contrast to $[MoOCl(CN\text{-}t\text{-}Bu)_4]BPh_4$, where the luminescence spectra provide essential additional information.

The luminescence spectra as a function of pressure in Fig. 5 show the most pronounced differences between the two complexes in Scheme 1. For $[MoOCl(CN\text{-}t\text{-}Bu)_4]BPh_4$ in Fig. 5a, the energy of the luminescence maximum increases with pressure between atmospheric pressure and approximately 25 kbar, corresponding to a blue shift. No blue-shift has been observed before in the pressure-dependent luminescence spectra of metal-oxo complexes,

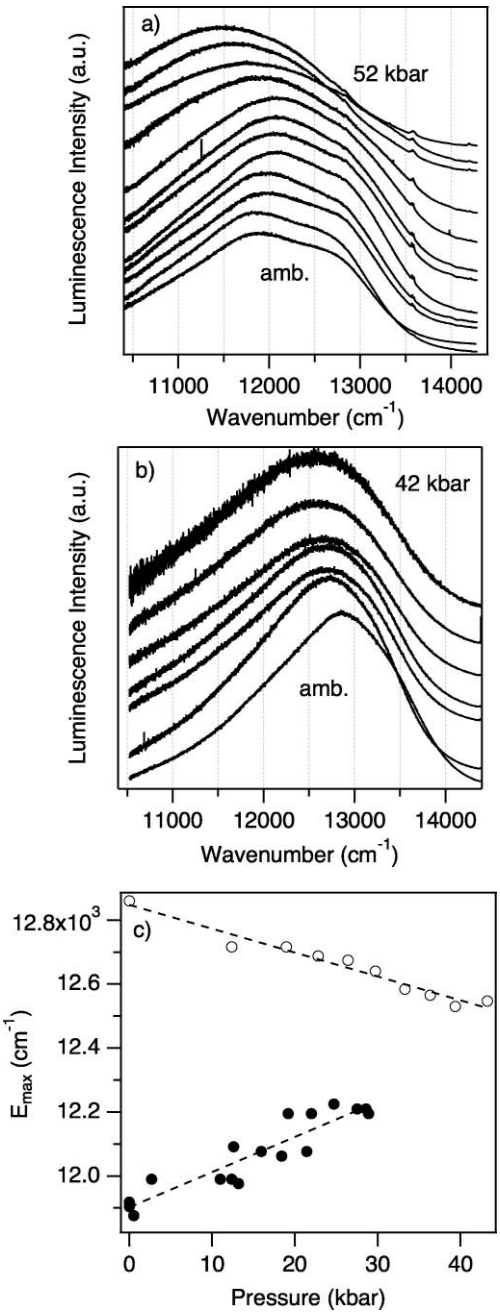

Fig. 5 Pressure-dependent luminescence spectra at room temperature. (a) $[MoOCl(CN\text{-}t\text{-}Bu)_4]BPh_4$. (b) $[MoOF(pyridine)_4]BPh_4$. (c) Position of the luminescence band maxima as a function of pressure. Solid circles: $[MoOCl(CN\text{-}t\text{-}Bu)_4]BPh_4$. Open circles: $[MoOF(pyridine)_4]BPh_4$.

but it is not unexpected for $[MoOCl(CN\text{-}t\text{-}Bu)_4]^+$, given the strong π-acceptor character of the isocyanide ligands. The luminescence spectra of $[MoOF(pyridine)_4]BPh_4$ in Fig. 5b show a red shift of the luminescence maximum as pressure increases. The luminescence maxima are summarized in Fig. 5c, clearly showing the qualitative trends and pressure-induced shifts of the band maxima of $+12\ cm^{-1}\ kbar^{-1}$ and $-8\ cm^{-1}\ kbar^{-1}$ for $[MoOCl(CN\text{-}t\text{-}Bu)_4]BPh_4$ and $[MoOF(pyridine)_4]BPh_4$, respectively.

Fig. 6 summarizes the pressure-dependent behavior of the molybdenum(IV)-oxo Raman frequencies and the luminescence maximum for $[MoOCl(CN\text{-}t\text{-}Bu)_4]BPh_4$. Two unusual phenomena, the nonlinear variation of the molybdenum(IV)-oxo Raman frequency and the change from blue- to red-shifted luminescence maxima, occur in the same pressure range above approximately 30 kbar and both changes are completely reversible once pressure is released, as is the Raman effect for the rhenium(V) mono-oxo complexes reported before.[13] The Raman band corresponding to the metal-oxo mode becomes broad at pressures above 30 kbar, indicating the presence of inequivalent metal-oxo bonds, most likely as a consequence of small pressure gradients throughout the sample crystal. Nevertheless, the maximum of the broad Raman peak clearly shifts to lower frequency as pressure increases, as illustrated in Fig. 6a. No change of the direction of the pressure-induced shift of the luminescence maximum has been reported before for any metal-oxo complex, and it is exceptional among all the luminescent transition metal complexes for which pressure-dependent data are reported in the literature.[36,37] Corresponding spectroscopic results for $[MoOF(pyridine)_4]BPh_4$ are given in Fig. S3, ESI† and do not show any significant deviation from linear shifts. All pressure effects are larger by at least one order of magnitude than the spectroscopic changes with temperature, as documented in the ESI.†

The sign of the shift of the luminescence maxima in Fig. 5c can be rationalized from the nature of the d_{xy} HOMO and $d_{xz,yz}$ LUMO of the two complexes by qualitatively considering the effect of a bond length decrease. These orbitals are calculated with DFT and shown in Fig. 7 and 8 for $[MoOCl(CN\text{-}t\text{-}Bu)_4]^+$ and $[MoOF(pyridine)_4]^+$, respectively. The calculated orbitals confirm the d–d character of the lowest-energy electronic transition. Fig. 7 clearly shows that the HOMO of $[MoOCl(CN\text{-}t\text{-}Bu)_4]^+$ is π-bonding for the four Mo–C bonds, corresponding to the main amplitude of this orbital. In contrast, the LUMO involves mainly the Mo–oxo and Mo–Cl bonds, with antibonding π* character. As these bonds shorten, the energy of the π-bonding HOMO decreases and the energy of the π* LUMO increases, leading to a blue-shift of the lowest-energy electronic transition, as observed for the luminescence maximum. The dominant progression in the low-temperature spectrum in Fig. 2 is only barely resolved at room temperature, and therefore the effect of pressure on the vibronic structure can be characterized only qualitatively. The first member is discernible as a shoulder at approximately 13000 cm^{-1} at ambient pressure and the second member corresponds to the band maximum. The intensity ratio of these two bands does not change as pressure increases, in contrast to *trans*-dioxo complexes of rhenium(V), where significant intensity gains for the high-energy members of the main progression were observed.[9,10,12] At pressures higher than 25 kbar, a strong red shift of the luminescence band maximum is observed, as illustrated in Fig. 6b. This effect can not be rationalized from Fig. 7 alone and will be discussed in the following section. The pressure-dependent luminescence behavior of $[MoOF(pyridine)_4]BPh_4$ is easily rationalized from the HOMO and LUMO in Fig. 8. The observed red-shift of

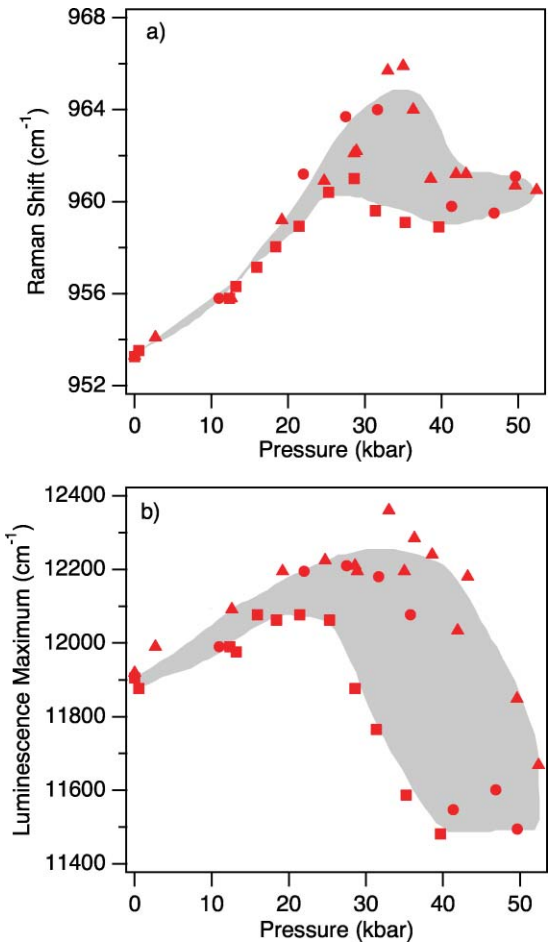

Fig. 6 (a) Raman band maxima for the Mo–oxo stretching mode of $[MoOCl(CN\text{-}t\text{-}Bu)_4]BPh_4$ as a function of pressure. (b) Luminescence band maxima of $[MoOCl(CN\text{-}t\text{-}Bu)_4]BPh_4$ as a function of pressure. Triangles, squares and circles denote two different series of experiments.

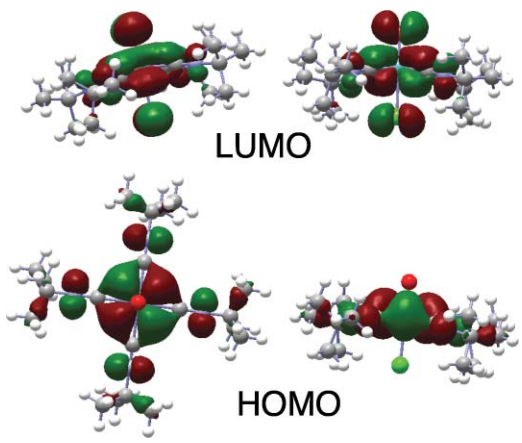

Fig. 7 DFT-calculated molecular orbitals. HOMO (bottom) and LUMO (top) of $[MoOCl(CN\text{-}t\text{-}Bu)_4]^+$. The HOMO is viewed along the Mo–oxo bond (left) and with the Mo–oxo bond vertically oriented (right). The Mo–oxo bond is vertically oriented for both views of the LUMO.

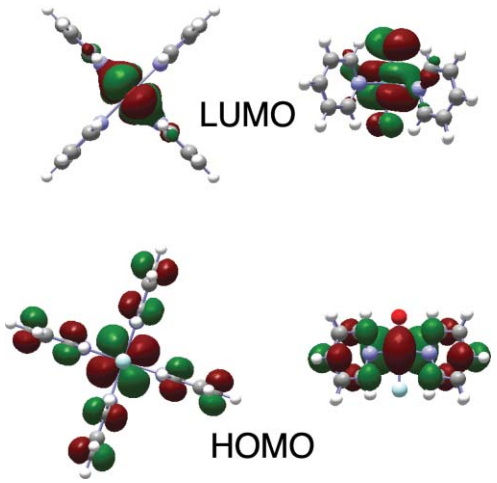

Fig. 8 DFT-calculated molecular orbitals. HOMO (bottom) and LUMO (top) of $[MoOF(pyridine)_4]^+$. Views are given along the Mo–oxo bond (left) and with the Mo–oxo bond vertically oriented (right).

-8 cm^{-1} $kbar^{-1}$ is similar in magnitude to those reported for several *trans*-dioxo complexes of rhenium(V) with ethylenediamine ligands,[10] but it is smaller than the red shift of -16 cm^{-1} $kbar^{-1}$ for *trans*-$[ReO_2(pyridine)_4]^+$.[12] In this case, the energy of the π^* LUMO again increases as the Mo–oxo and Mo–F bonds are compressed at high pressure, and the energy of the π^* HOMO also increases. This latter increase dominates, as it involves exclusively metal–ligand single bonds, and the result is a red shift of the luminescence band maximum. The pressure dependent luminescence spectra reveal therefore discernible differences between the two complexes studied here, caused by the metal–ligand single bonds in the plane perpendicular to the molybdenum(IV)-oxo bond. This difference is not visible from the ambient pressure luminescence spectra in Fig. 2 and 3 with maxima at very similar energies.

4. Discussion

4.1 Low-temperature luminescence spectroscopy

The low-temperature luminescence spectra in Fig. 2 and 3 provide sufficient information to analyze the main structural changes between the ground and emitting states of the two molybdenum(IV) oxo complexes studied here. Calculated luminescence spectra based on harmonic potential energy surfaces for both the ground and emitting states are used to determine these structure changes.

Using the three different metal–ligand stretching frequencies $h\omega_{MoO}$, $h\omega_{MoL}$ and $h\omega_{MoX}$, where L and X denote the ligands in the xy plane and *trans* to the oxo ligand, respectively, the ground-state potential-energy surface E_{GS} is given by:

$$E_{GS} = \frac{1}{2}\left(\hbar\omega_{MoO}Q_{MoO}^2 + \hbar\omega_{MoL}Q_{MoL}^2 + \hbar\omega_{MoX}Q_{MoX}^2\right) \quad (1)$$

The emitting state potential energy surface E_{ES} is given by:

$$E_{ES} = \frac{1}{2}\begin{pmatrix}\hbar\omega_{MoO}\left(Q_{MoO} - \Delta_{MoO}\right)^2 + \hbar\omega_{MoL}\left(Q_{MoL} - \Delta_{MoL}\right)^2 \\ +\hbar\omega_{MoX}\left(Q_{MoX} - \Delta_{MoX}\right)^2\end{pmatrix} \quad (2)$$

We use identical vibrational frequencies $h\omega_i$ in wavenumber (cm^{-1}) units for the ground and emitting states, as determined from Raman spectra and summarized in Table 3. The emitting state potential energy surface is offset by Δ_i (in dimensionless units) along the three normal coordinates in eqn (1) and 2. In our model, all offsets along other coordinates are zero. The luminescence spectrum for a transition between states defined by the potential energy surfaces in eqn (1) and (2) is:[38–40]

$$I(\omega) = C\omega^3 \int_{-\infty}^{\infty} e^{i\omega t} e^{\sum_i -\left[\frac{\Delta_i^2}{2}\left(1-e^{-i\omega_i t}\right)-\frac{i\omega_i t}{2}\right] - iE_{00}t - \Gamma^2 t^2} \mathrm{d}t \quad (3)$$

The electronic origin of the luminescence transition E_{00} is estimated from experimental absorption and luminescence spectra and the horizontal offsets Δ_i were treated as adjustable parameters. The damping factor Γ in wavenumber (cm^{-1}) units is chosen to approximately reproduce the observed vibronic bandwidths. This simple model leads to calculated spectra in good agreement with the experimental data, as illustrated in Fig. 2 and 3.

Significant deviations from a harmonic ground-state potential energy surface appear to be absent, in contrast to complexes of the 5d metals, where model calculations based on harmonic potential energy surfaces often do not lead to a quantitative agreement with the experimental spectrum.[7,41] All model parameters are summarized in Table 4. Both complexes show an offset along the Mo–oxo stretching coordinate with a positive bond length change along the metal-oxo coordinate, corresponding to a longer Mo–oxo bond in the emitting state. This is the case for all metal-oxo and *trans*-dioxo complexes studied and it is also intuitively obvious from the metal-oxo π^* character of the LUMO ($d_{xz,yz}$) orbitals shown in Fig. 7 and 8. In addition, the published low-temperature absorption spectrum of $[MoOCl(CN\text{-}t\text{-}Bu)_4]BPh_4$ and our own measurement presented in Fig. S1, ESI† show that the Mo–oxo frequency decreases to 800 cm^{-1} in the emitting state, confirming the presence of a weaker and therefore longer bond. The situation is less clear-cut for the Mo-isocyanide frequency. Since this is a π-acceptor ligand, we expect a bonding interaction between the ligator atom and the metal center for the HOMO (d_{xy}) orbital in this compound. Removing an electron in order to obtain the LUMO electron configuration leads to a weakening of this bond in the emitting state and a frequency decrease from 441 cm^{-1} in the ground state to 350 cm^{-1} in the emitting state is observed for the Mo-isocyanide stretching mode. In contrast, for many compounds with π-donor ligands, a frequency increase is actually observed in the emitting state, indicating that the offset Δ_{ML} is negative.[7]

The offset along the molybdenum(IV)-oxo normal coordinate is smaller for $[MoOF(pyridine)_4]^+$ than for $[MoOCl(CN\text{-}t\text{-}Bu)_4]^+$. An

Table 4 Parameters used for the calculation of the luminescence spectra in Fig. 2 and 3 using eqn (1)–(3)

Parameter	$[MoOCl(CN\text{-}t\text{-}Bu)_4]BPh_4$	$[MoOF(pyridine)_4]BPh_4$
E_{00}/cm^{-1}	12690	13420
$h\omega_{MoO}$ (cm^{-1}), Δ_{MoO} (dimensionless)	954, 1.72	953, 0.7
$h\omega_{MoF}$ (cm^{-1}), Δ_{MoF} (dimensionless)	n/a	475, 1.65
$h\omega_{MoCN\text{-}t\text{-}Bu}$ (cm^{-1}), $\Delta_{MoCN\text{-}t\text{-}Bu}$ (dimensionless)	441, 0.95	n/a
Γ (cm^{-1})	170	140

important offset along a coordinate with a frequency of 475 cm^{-1} is observed for $[MoOF(pyridine)_4]^+$. This mode corresponds to the Mo–F stretching vibration, as listed in Table 3. The analysis of the luminescence spectrum in Fig. 3 shows the unique effects caused by the fluoride ligand *trans* to the molybdenum(IV)-oxo multiple bond: it competes very efficiently with the oxo ligand for bonding electron density, leading to an unusually small value of Δ_{MoO}. Fig. 3 shows the first luminescence spectrum of a metal-oxo complex with a fluoride ligand, indicating a new, large variation of the emitting state properties *via* the ligand *trans* to the metal-oxo multiple bond. The Mo-pyridine stretching mode is not expected to form a long progression and no vibronic features corresponding to this mode are resolved in the luminescence spectrum in Fig. 3, as the frequency of this mode is calculated to be lower than 200 cm^{-1}. The experimental spectrum shows many partially overlapping bands in the region between 150 and 250 cm^{-1} and an unambiguous assignment of any single peak to this mode is not possible. In addition, the DFT calculations illustrate that only a weak π interaction occurs in the HOMO between the metal-centered d_{xy} and pyridine-centered π orbitals, and no interaction at all is calculated for the LUMO, as illustrated in Fig. 7 and 8. Therefore only a very small offset Δ_{MoL} is expected, leading to a short progression that is hidden within the bandwidth of the vibronic bands in Fig. 3.

For $[MoOCl(CN\text{-}t\text{-}Bu)_4]BPh_4$, a vibronic interval of 920 ± 10 cm^{-1} is observed in the experimental luminescence spectrum in Fig. 2. We observe three intervals, in contrast to the literature, where only the highest-energy peak[18] or only a single interval between the first two members of the dominant vibronic progression[17] are reported. The observed progression interval does not correspond exactly to the ground-state molybdenum(IV)-oxo stretching frequency of 954 cm^{-1} in Table 3. This difference is a manifestation of the missing mode effect (MIME)[42-44] due to nonzero Δ_i values for more than one normal coordinate, but only a single resolved vibronic progression. A calculated spectrum using only the 954 cm^{-1} mode leads to a significantly inferior agreement. The Mo-isocyanide stretching mode with a frequency of 441 cm^{-1} has to be included to reproduce the progression interval to understand the observed MIME interval $\hbar\omega_M$ of 920 cm^{-1}. In our model, this interval is given by:[44]

$$\hbar\omega_M = \frac{\sum_k \hbar\omega_k^2\Delta_k^2 + 4\Gamma^2}{\sum_k \hbar\omega_k\Delta_k^2 n_k} \quad (4)$$

Using eqn(4) and the 954 and 441 cm^{-1} frequencies with their offsets Δ_k given in Table 4 and $n_k = 1$, we calculate a $\hbar\omega_M$ value of 926 cm^{-1}, in excellent agreement with the experiment. The addition of the low-frequency Mo–Cl stretching mode with a nonzero Δ_{MoCl} could further decrease this calculated MIME interval, but since we do not observe this mode directly in the luminescence spectrum, it was not included in the analysis. The ambient pressure luminescence spectra allow the characterization of the emitting state and several differences between the two complexes are revealed by the comparisons of experimental and calculated luminescence spectra and qualitative molecular orbital arguments based on the DFT calculations.

4.2 Pressure effects on Raman and luminescence spectra of $[MoOCl(CN\text{-}t\text{-}Bu)_4]BPh_4$

The Raman and luminescence spectra at variable pressure in Fig. 4 and 5 show obvious differences between the two complexes, most notably the different directions of the pressure-induced shifts of the luminescence band maxima in Fig. 5c. Previous work on *trans*-dioxo complexes of rhenium(V) has shown that a red shift is observed for the luminescence band maxima of pyridine complexes.[12] A shift in the same direction is observed in Fig. 5b for $[MoOF(pyridine)_4]BPh_4$. In contrast, a blue shift is observed for the isocyanide complex. These shifts can be understood in terms of small bond length decreases with increasing pressure. Multiple metal-oxo bond lengths show the smallest change as pressure increases, illustrated by the pressure-dependent luminescence spectra of *trans*-dioxo complexes, where a red shift of the luminescence maximum is observed as pressure increases. Their π^* LUMO ($d_{xz,yz}$) is less destabilized than their π^* HOMO (d_{xy}), rationalizing the red shift as a consequence of the π^* nature of the HOMO orbital and the stronger influence of pressure on single bonds than on stronger multiple metal-oxo bonds. Based on the same argument, a blue shift is expected for a complex with π acceptor ligands in the xy plane, due to the π bonding HOMO orbital whose energy decreases with increasing pressure.

The pressure-induced changes of the Raman frequencies below 25 kbar are similar for the two compounds, illustrated by the increases of the metal-oxo frequencies by +0.24 cm^{-1} $kbar^{-1}$ and +0.18 cm^{-1} $kbar^{-1}$ for $[MoOCl(CN\text{-}t\text{-}Bu)_4]BPh_4$ and $[MoOF(pyridine)_4]BPh_4$, respectively, as shown in Fig. 4 and Table 3. The ESI† contains other regions of the Raman spectra measured at variable pressure in Fig. S2. At pressures above 25 kbar, the $[MoOCl(CN\text{-}t\text{-}Bu)_4]BPh_4$ complex shows an unusual change of the Mo–oxo stretching peak, illustrated in Fig. 4a. The maximum of the Raman peak shifts to lower frequency and the peak becomes much broader. This is the only peak in the Raman spectrum with such an unusual behavior. An intuitively appealing reason for the Mo–oxo frequency decrease is the competition between the Mo–oxo and Mo–chloride bonds. The Mo–Cl single bond length is likely to change by a larger amount than the metal-oxo distance as pressure increases. These unequal changes lead to a more symmetric electron density distribution along the Cl–Mo–O axis and consequently to a weaker Mo–oxo bond. The asymmetry of the electron distribution along this axis can be clearly seen from the HOMO and LUMO plots in Fig. 7 and 8. The effect of the Mo–Cl bond length on the Mo–oxo vibrational frequency and bond length has been explored with DFT calculations as illustrated in Fig. S7, ESI.† The Mo–Cl bond length was shortened and the molecular structure optimized. A shorter Mo–Cl bond length leads to an increase of the Mo–oxo vibrational frequency and bond length, qualitatively rationalizing the observed decrease of the metal oxo frequencies with increasing pressure in mono-oxo complexes of both molybdenum(IV), shown in Fig. 4a, and rhenium(V).[13] The broadening of the Raman band in Fig. 4a indicates that inhomogeneous broadening occurs, likely due to structural changes other than Mo–oxo bond shortening. Angular changes are likely candidates leading to inhomogeneous broadening, and one such angle change will be studied to rationalize the unusual shift of the luminescence maximum in Fig. 6b. Additional indirect evidence for a large effect of pressure

on the Mo–Cl bond is provided by the barely resolved vibronic structure in the luminescence spectra in Fig. 5a. The intensity ratio of the first two peaks appears to be pressure-independent within the precision of our experiment, indicating little or no change of Δ_{MoO} with increasing pressure, likely due to the larger compression of the Mo–Cl bond, in contrast to *trans*-dioxo complexes of rhenium(V), where the intensity ratio of the first two peaks changes significantly as Δ_{OReO} decreases with pressure.[9,10] The bonding situation along the OMoF axis for $[MoOF(pyridine)_4]BPh_4$ does not lead to a pressure-induced deviation from a linear increase of the Mo–oxo stretching frequency in the pressure range studied here.

The luminescence spectra of $[MoOCl(CN\text{-}t\text{-}Bu)_4]BPh_4$ also show an obvious change in the same pressure range as the Mo–oxo Raman frequency. The blue shift of the luminescence band maximum at pressures below 25 kbar is easily understood in qualitative terms from the electron configurations of the ground and emitting states. Density functional theory is used to rationalize the observed shifts in more detail. External pressure leads to small decreases of bond lengths, explored through DFT calculations for each category of metal–ligand bonds.

Fig. 9 shows calculated variations of the HOMO and LUMO energies and of the lowest-energy absorption maxima. The lengths of the Mo–Cl and Mo–C single bonds are shortened by up to 5%, a change larger than induced by our highest experimental pressure. Fig. 9a shows that the energies of both HOMO and LUMO orbitals increase as the Mo–Cl bond length decreases. The $d_{xz,yz}$ LUMO is strongly π antibonding and is more strongly destabilized as the chloro π donor ligand approaches than the d_{xy} HOMO, which is not significantly contributing to the Mo–Cl bond. This is clearly illustrated by the calculations in Fig. 9a, leading to a HOMO–LUMO energy difference that increases as the Mo–Cl bond length decreases, corresponding to an increase of the external pressure. The effects of Mo–C bond shortening on the same orbital energies are shown in Fig. 9b. The HOMO orbital is π bonding, confirmed by its strong decrease in energy as the isocyanide ligands move closer to the molybdenum(IV) center. The calculations clearly illustrate the π acceptor character of the isocyanide ligands. The energy of the LUMO orbital also decreases, but to a lesser extent because most of the metal electron density along the z axis is used for the metal-oxo multiple bond. This bond length change therefore also leads to an increase of the HOMO–LUMO energy difference, as illustrated in Fig. 9b.

TD-DFT calculations provide calculated absorption band maxima of the lowest triplet excited state. The calculated absorption energy is within 1000 cm^{-1} of the experimental band maximum shown in the literature[18] and in Fig. S1a, ESI,† an excellent agreement in view of many simplifying model assumptions, such as the neglect of spin–orbit coupling in our calculations. The energies of these absorption transitions are shown in Fig. 9c for Mo–Cl and 9d for Mo–C. Both bond length decreases lead to energy increases of the absorption maximum. These calculations indicate that external pressure leads to a blue shift of the lowest-energy electronic transition, in agreement with the luminescence spectra at pressures below 25 kbar in Fig. 5.

Effects other than bond length variations cause the red shift of the luminescence maximum at pressures higher than 25 kbar, illustrated in Fig. 6b. The most obvious structural change to be studied is the O–Mo–C angle α, shown in Fig. 10. This angle

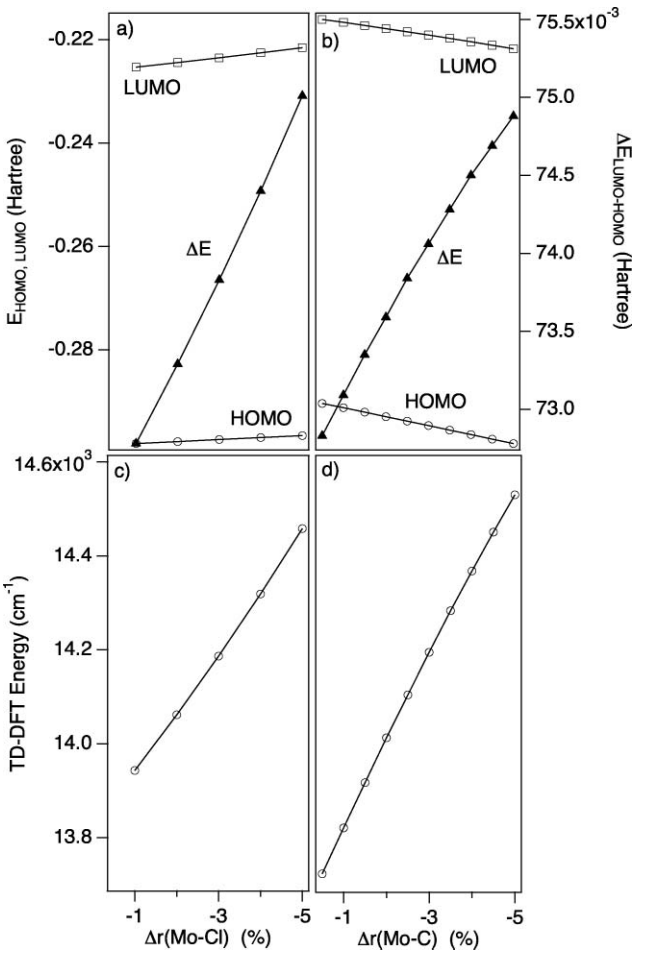

Fig. 9 (a) Calculated (DFT) variations of the HOMO (circles) and LUMO (squares) orbital energies as the Mo–Cl distance is shortened from its equilibrium value. (b) Calculated variations of the HOMO and LUMO orbital energies as the Mo–C(CN-*t*-Bu_4) distance is shortened from its equilibrium value. The energy difference between the orbitals (solid triangles) increases as bonds are shortened. (c,d) Calculated (TDDFT) variation of the absorption band maximum for the transition to the lowest triplet excited state.

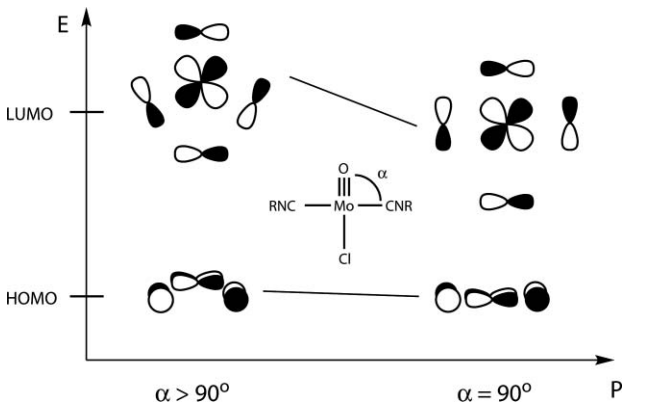

Fig. 10 Schematic view of the HOMO and LUMO energies as a function of the O–Mo–C angle α.

is 95° in the experimental structure[18] and 90° in *trans*-dioxo complexes.[45] As the Mo–Cl bond length decreases, the angle α

can be expected to decrease, as indicated by theoretical studies on E=ML$_4$X complexes.[22-25] The angle α is largest for complexes without a ligand *trans* to the multiple bond.[22,25] The qualitative orbitals in Fig. 10 show that the LUMO energy decreases strongly as α decreases, a structural change likely to occur at high pressure with a shorter and stronger Mo–Cl bond. This decrease is due to the significant change in angular overlap between the $d_{xz,yz}$ metal and π(z)* isocyanide-centered orbitals. The change in overlap is smaller for the HOMO orbital, involving d_{xy}(Mo) and π(x,y)* isocyanide-centered orbitals, as schematically shown in Fig. 10.

Fig. 11 summarizes the DFT calculations for the variation of the angle α. Fig. 11a shows that the LUMO energy decreases more strongly than the HOMO energy, leading to an overall decrease of the energy difference and therefore to a decrease of the lowest-energy absorption maximum, as shown in Fig. 11b. This structural change leads to a shift of the lowest-energy electronic transition in the opposite direction to those in Fig. 9. A decrease of α by 5° results in a decrease of the calculated transition energy by approximately 1000 cm^{-1}. This shift is comparable in magnitude to combined changes on the order of 1% for the Mo–Cl and Mo–C bond lengths. The combined effect of these opposing trends can lead to a blue shift ***or*** to a red shift. We conclude that [MoOCl(CN-*t*-Bu)$_4$]BPh$_4$ is a rare case where different effects dominate at pressures above and below 25 kbar, leading to the change of direction for the pressure-induced shift of the luminescence band maximum. This behavior is rare, but has been observed before for Cr^{4+} ions doped into distorted tetrahedral sites of Y_2SiO_5, where a blue shift of the luminescence maximum is observed between ambient pressure and approximately 40 kbar, followed by a red shift at higher pressures.[46] This change was interpreted as arising from a competition between pressure-induced increases of the tetrahedral ligand-field strength and pressure-induced decreases of the parameters defining deviations from perfect tetrahedral symmetry,[46] a situation qualitatively similar to the effect presented in Fig. 5a.

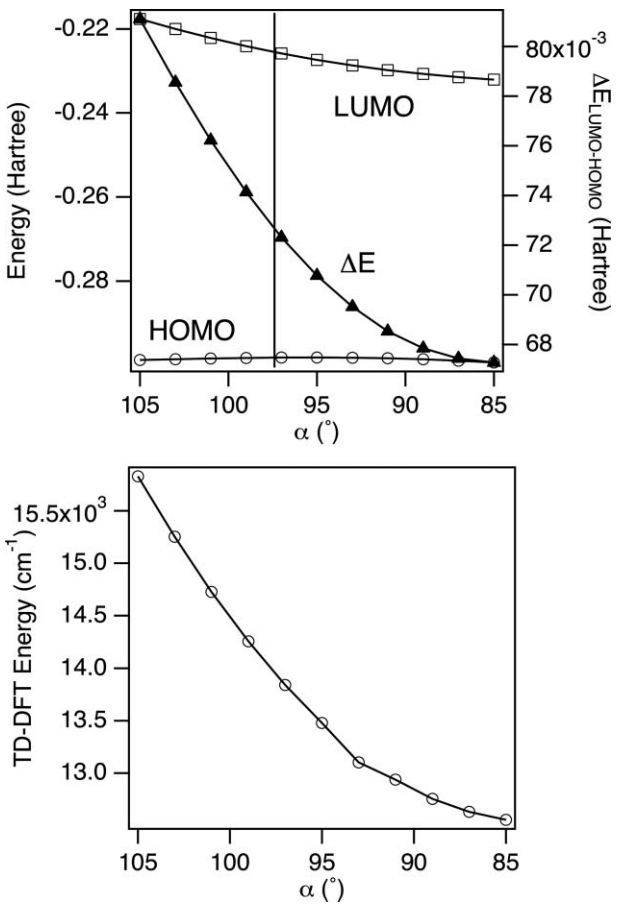

Fig. 11 (a) Calculated (DFT) variations of the HOMO (circles) and LUMO (squares) orbital energies as a function of O–Mo–C(CN-*t*-Bu$_4$) angle α. The vertical line denotes the experimental angle at ambient pressure. The energy difference between these two orbitals decreases with decreasing α (solid triangles) (b) Calculated (TDDFT) energy of the lowest-energy absorption transition as a function of the angle α.

This first study on the pressure-dependent luminescence and Raman spectra of molybdenum(IV) oxo complexes reveals a rich variety of phenomena, indicating intriguing possibilities for further exploration by specific variations of structural parameters such as ligand-metal–ligand bond angles of these versatile luminophores.

Acknowledgements

We thank Professor Matthias Ernzerhof (Université de Montréal) for guidance with the DFT calculations, Daniel Gareau (Université de Montréal) for technical help and the Natural Sciences and Engineering Research Council (Canada) for financial support.

References

1 J. R. Winkler and H. B. Gray, *J. Am. Chem. Soc.*, 1983, **105**, 1373.
2 J. R. Winkler and H. B. Gray, *Inorg. Chem.*, 1985, **24**, 346.
3 V. M. Miskowski, H. B. Gray and M. D. Hopkins, in *Adv. in Trans. Met. Coord. Chem.*, ed. C.-M. Che and V. W.-W. Yam, JAI Press, Greenwich, CT, Editon edn, 1996, vol. 1, pp. 159.
4 M. D. Newsham, E. P. Giannelis, T. J. Pinnavaia and D. G. Nocera, *J. Am. Chem. Soc.*, 1988, **110**, 3885.
5 H. H. Thorp, C. V. Kumer, N. J. Turro and H. B. Gray, *J. Am. Chem. Soc.*, 1989, **111**, 4364.
6 C.-M. Che, V. W.-W. Yam, K.-C. Cho and H. B. Gray, *J. Chem. Soc., Chem. Commun.*, 1987, 948.
7 C. Savoie and C. Reber, *Coord. Chem. Rev.*, 1998, **171**, 387.
8 C. Savoie and C. Reber, *J. Am. Chem. Soc.*, 2000, **122**, 844.
9 J. K. Grey, M. Triest, I. S. Butler and C. Reber, *J. Phys. Chem. A*, 2001, **105**, 6269.
10 J. K. Grey, I. S. Butler and C. Reber, *J. Am. Chem. Soc.*, 2002, **124**, 11699.
11 J. K. Grey, I. S. Butler and C. Reber, *Inorg. Chem.*, 2004, **43**, 5103.
12 J. K. Grey, I. S. Butler and C. Reber, *Can. J. Chem.*, 2004, **82**, 1083.
13 J. K. Grey, M. Marguerit, I. S. Butler and C. Reber, *Chem. Phys. Lett.*, 2002, **366**, 361.
14 S. E. Bailey, R. A. Eikey, M. M. Abu-Omar and J. I. Zink, *Inorg. Chem.*, 2002, **41**, 1755.
15 M. D. Hopkins, V. M. Miskowski and H. B. Gray, *J. Am. Chem. Soc.*, 1986, **108**, 6908.
16 U. Oetliker, C. Savoie, S. Stanislas, C. Reber, F. Connac, A. L. Beauchamp, F. Loiseau and M. Dartiguenave, *Chem. Commun.*, 1998, 657.
17 R. A. Isovitsch, A. S. Beadle, F. R. Fronczek and A. W. Maverick, *Inorg. Chem.*, 1998, **37**, 4258.
18 R. E. Da Re and M. D. Hopkins, *Inorg. Chem.*, 2002, **41**, 6973.
19 A. S. Del Negro, Z. Wang, C. J. Seliskar, W. R. Heineman, B. P. Sullivan, S. E. Hightower, T. L. Hubler and S. A. Bryan, *J. Am. Chem. Soc.*, 2005, **127**, 14978.
20 K. Mersmann, A. Hauser, N. Lehnert and F. Tuczek, *Inorg. Chem.*, 2006, **45**, 5044.
21 C. D. Brondino, M. G. Rivas, M. J. Romão, J. J. G. Moura and I. Moura, *Acc. Chem. Res.*, 2006, **39**, 788.

22 P. D. Lyne and D. M. P. Mingos, *J. Chem. Soc., Dalton Trans.*, 1995, 1635.
23 P. Mountford and D. Swallow, *J. Chem. Soc., Chem. Commun.*, 1995, 2357.
24 N. Kaltsoyannis and P. Mountford, *J. Chem. Soc., Dalton Trans.*, 1999, 781.
25 C. E. Schäffer, C. Anthon and J. Bendix, *Coord. Chem. Rev.*, 2009, **253**, 575.
26 M. Brorson and C. E. Schäffer, *Acta Chem. Scand., Ser. A*, 1986, **40a**, 358.
27 J. Bendix and A. Bøgevig, *Inorg. Chem.*, 1998, **37**, 5992.
28 J. Bendix and A. Bøgevig, *Acta Crystallogr., Sect. C: Cryst. Struct. Commun.*, 1998, **54**, 206.
29 C. K. Johnson, *ORTEP-II*. Report ORNL-5138 Oak Ridge National Laboratory, Tennessee, USA, 1976.
30 M. J. Davis and C. Reber, *Inorg. Chem.*, 1995, **34**, 4585.
31 G. J. Piermarini, S. Block, J. D. Barnett and R. A. Forman, *J. Appl. Phys.*, 1975, **46**, 2774.
32 M. J. Frisch, G. W. Trucks, H. B. Schlegel, G. E. Scuseria, M. A. Robb, J. R. Cheeseman, V. G. Zakrzewski, J. A. Montgomery Jr., R. E. Stratmann, J. C. Burant, S. Dapprich, J. M. Millam, A. D. Daniels, K. N. Kudin, M. C. Strain, O. Farkas, J. Tomasi, V. Barone, B. Mennucci, M. Cossi, C. Adamo, J. Jaramillo, R. Cammi, C. Pomelli, J. Ochterski, G. A. Petersson, P. Y. Ayala, K. Morokuma, D. K. Malick, A. D. Rabuck, K. Raghavachari, J. B. Foresman, J. V. Ortiz, Q. Cui, A. G. Baboul, S. Clifford, J. Cioslowski, B. B. Stefanov, G. Liu, A. Liashenko, P. Piskorz, I. Komaromi, R. Gomperts, R. L. Martin, D. J. Fox, T. Keith, M. A. Al-Laham, C. Y. Peng, A. Nanayakkara, M. Challacombe, P. M. W. Gill, B. Johnson, W. Chen, M. W. Wong, J. L. Andres, C. Gonzalez, M. Head-Gordon, E. S. Replogle and J. A. Pople, Gaussian, Inc., Pittsburgh PA, Editon edn, 2001.
33 P. Hummel, J. R. Winkler and H. B. Gray, *Dalton Trans.*, 2006, 168.
34 C. S. Johnson, C. Mottley and J. T. Hupp, *Inorg. Chem.*, 1992, **31**, 5143.
35 J. Bendix, unpublished data.
36 K. L. Bray, *Top. Curr. Chem.*, 2001, **213**, 1.
37 J. K. Grey and I. S. Butler, *Coord. Chem. Rev.*, 2001, **219–221**, 713.
38 E. J. Heller, *Acc. Chem. Res.*, 1981, **14**, 368.
39 J. I. Zink, *Coord. Chem. Rev.*, 2001, **211**, 69.
40 J. I. Zink and K.-S. K. Shin, *Adv. Photochem.*, 1991, 119.
41 J. Landry-Hum, V. Tessier, M. Ernzerhof and C. Reber, *Coord. Chem. Rev.*, 2002, **233–234**, 63.
42 L. W. Tutt, D. Tannor, E. J. Heller and J. I. Zink, *Inorg. Chem.*, 1982, **21**, 3858.
43 L. W. Tutt and J. I. Zink, *J. Am. Chem. Soc.*, 1986, **108**, 5830.
44 L. W. Tutt, J. I. Zink and E. J. Heller, *Inorg. Chem.*, 1987, **26**, 2158.
45 S. Bélanger and A. L. Beauchamp, *Inorg. Chem.*, 1996, **35**, 7836.
46 Y. Shen, T. Riedener and K. L. Bray, *Phys. Rev. B: Condens. Matter Mater. Phys.*, 2000, **61**, 9277.